

Hole mobility enhancement by chain alignment in nanoimprinted poly(3-hexylthiophene) nanogratings for organic electronics

Min Zhou and Mukti Aryal

Department of Electrical Engineering, The University of Texas at Dallas, Richardson, Texas 75080

Kamil Mielczarek and Anvar Zakhidov

Department of Physics, The University of Texas at Dallas, Richardson, Texas 75080

Walter Hu^{a)}

Department of Electrical Engineering, The University of Texas at Dallas, Richardson, Texas 75080

(Received 7 July 2010; accepted 7 September 2010; published 1 December 2010)

The authors report that the poly(3-hexylthiophene-2,5-diyl) (P3HT) nanogratings shaped by nanoimprint lithography show enhanced hole mobility and strong anisotropy of conductance due to nanoimprint-induced three-dimensional polymer chain alignment. Field effect transistors were fabricated using these nanogratings and device measurements show a hole mobility of $0.03 \text{ cm}^2/\text{V s}$ along the grating direction, which is about 60 times higher than that of nonoptimized thin film transistors. Organic photovoltaic devices (OPV) were made using the P3HT nanograting with infiltration of [6,6]-phenyl-C61-butyric acid methyl ester. Compared to similar bilayer and bulk heterojunction devices, the nanoimprinted OPV shows improved device performance. © 2010 American Vacuum Society. [DOI: 10.1116/1.3501343]

I. INTRODUCTION

Organic electronics such as photovoltaic and thin film transistors (TFTs) using conjugated polymers have received increasing attention because of their low cost, flexibility, and light weight.^{1,2} However, the performance of organic devices is limited by the low charge mobility in organic semiconductors, which can be enhanced by controlling both the material morphology and the molecular or chain arrangement/orientation in the solid state.³ For example, the power conversion efficiency of organic photovoltaic (OPV) solar cells depends on fill factor (FF), short circuit current density (I_{sc}), and open circuit voltage (V_{oc}).⁴ Both FF and I_{sc} increase with higher charge carrier mobility,^{5,6} in particular, the hole mobility of the polymeric component. Hence, high carrier mobility values are desired for better power conversion efficiency. Since mobility in OPV and field effect transistors (FETs) can be increased significantly with ordered polymer chain alignment, many methods have been utilized to improve the crystallinity of poly(3-hexylthiophene-2,5-diyl) (P3HT), such as drop casting,⁷ electrospinning,⁸ surface treatment,⁹ thermal annealing,¹⁰ and vapor treatment.¹¹ These techniques have achieved some degree of chain ordering and some of them lead to improved device performance. However, it remains a great challenge for organic devices to achieve ultimate control of both film morphology and favorable molecular orientation and crystallinity.¹² When crystallinity and chain alignment are achieved within organic semiconducting nanowires/gratings, these nanogratings can provide a unique platform to study correlations among morphology, molecular orientation, and transport mechanism for

organic devices. Significant achievements have been reported in this direction and they are extensively discussed in a recent review article.³

Most previous organic nanowires were prepared using self-assembly methods or electrospinning. Although nanowires with well controlled crystallinity and even single crystalline wires can be obtained using these methods, it remains highly challenging for these methods to achieve precise dimensional control, on-chip alignment, and hybrid integration to make large scale devices/systems.³ An alternative approach to make similar nanowires without the aforementioned issues is “top-down” lithography. For example, nanoimprint lithography (NIL) has recently been demonstrated as an accurate and feasible method to make nanowires (both lateral and vertical chain alignments) in various semiconducting polymers.^{13–15} These nanowires have been successfully used in various applications, such as sensor, solar cells, and transistors. Importantly, the NIL method can simultaneously control both the structural dimensionality and the chain orientation within the nanostructures.^{13,16,17} Despite these emerging works, the comprehensive understanding of correlations of nanoimprint, three-dimensional (3D) polymer alignment, and carrier mobility is still limited. In our previous work, we have shown that nanoimprint lithography can induce three-dimensional and highly ordered chain alignments within P3HT nanostructures.¹⁷ For example, P3HT nanogratings have favorable vertical chain alignment and π -stacking along the grating direction. In this article, we demonstrate the use of nanoimprinted P3HT nanogratings in a back-gated field effect transistor and show that nanoconfinement induced 3D chain alignment in these nanowires has significantly enhanced the hole mobility by 60 times in comparison to nonimprinted TFT. We also fabricated P3HT/[6,6]-phenyl-C61-butyric acid methyl ester (PCBM) based

^{a)}Electronic mail: walter.hu@utdallas.edu

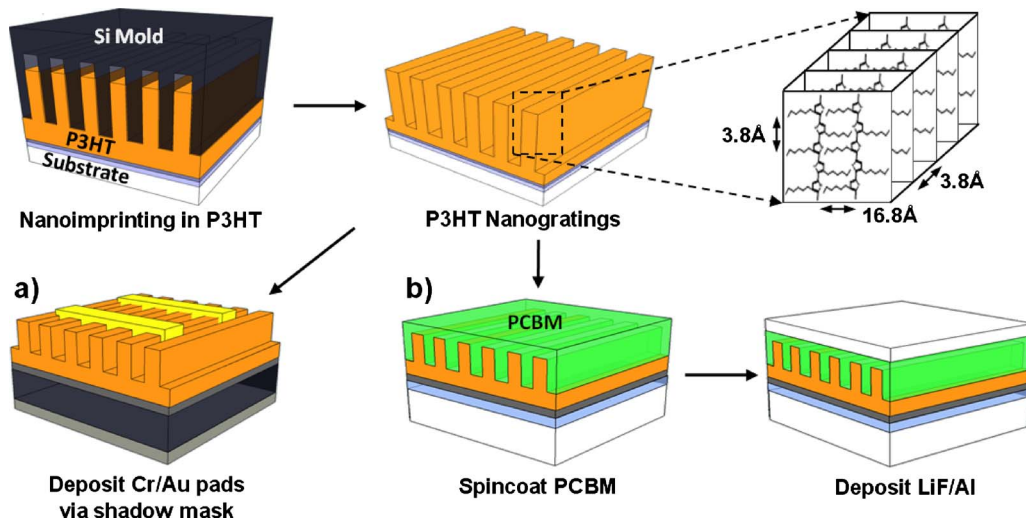


FIG. 1. (Color online) Schematic of the fabrication process of (a) nanograting field effect transistor and (b) nanograting solar cells. The cartoon of polymer chain orientation shows π -stacking in the lateral direction and backbone orientation in the vertical direction in P3HT nanogratings.

OPV devices using these nanogratings in comparison to bilayer and bulk heterojunction or blend devices. The high mobility enabled by the favorable 3D chain configuration contributes to the improved current density, fill factor, and efficiency of the nanoimprinted OPV.

II. DEVICE FABRICATIONS

Figure 1 shows the schematic of the fabrication process of nanograting FETs and OPV devices side by side. These two fabrication processes share some steps, such as spin coating and nanoimprinting of P3HT. Nanoimprinting creates polymer chain alignment, which is favorable to both devices as shown. FETs were fabricated using nanoimprinted P3HT gratings as channels to measure the hole mobility in comparison to nonimprinted TFT. All FETs have top contacts deposited by evaporation through a shadow mask and use a back gate configuration. FETs were fabricated on heavily doped *n*-type (100) Si wafer (0.002 Ω cm) substrates with 200 nm thick thermally grown silicon oxide as gate dielectric. 200 nm thick Al was deposited by an electron-beam evaporator on the backside of the Si substrates as a back gate electrode. Regio-regular P3HT (Sigma-Aldrich, Mn = 25 000–35 000 Da) in dichlorobenzene was spin coated on oxidized Si, followed by annealing at 150 $^{\circ}$ C for 5 min to obtain \sim 80 nm thick P3HT films. P3HT nanogratings were fabricated by nanoimprinting at 170 $^{\circ}$ C for 10 min at 50 bars and demolded at 70 $^{\circ}$ C. As shown in Fig. 2(a), the nanoimprinted gratings covering 200 mm² areas are about 150 nm in height, 65 nm in width, and 200 nm in pitch, with 20 nm thick residual layer. Cr/Au (20 nm/200 nm) pads as source and drain contacts were deposited sequentially by electron-beam evaporation and defined by a shadow mask with a channel length of 30 μ m and channel widths of 100 μ m on top of the P3HT nanogratings. The source/drain metal pads have two different orientations, e.g., along the grating direction for parallel devices and perpendicular to the grating direction for perpendicular devices [Fig. 2(b)]. For perpendicular

lar devices, the 20 nm thick residual layer connects the nanogratings. A set of TFT devices were also fabricated using nonimprinted P3HT films with three different thicknesses (20, 80, and 140 nm) for comparison. Among these three thicknesses of P3HT film, 20 and 80 nm are chosen to be equal to the residual layer thickness and starting film thickness of nanoimprinted FETs, respectively. Finally, the devices were annealed at 100 $^{\circ}$ C for 6–8 h in nitrogen environment to dedope oxygen before measurements.¹⁸ The electrical characterizations were performed using a Cascade Microtech probing station and a Keithley 4200 semiconductor characterization system at room temperature and ambient condition.

Figure 1(b) shows the fabrication process to make the nanograting P3HT/PCBM OPV devices using imprinted P3HT nanogratings on patterned indium tin oxide (ITO) (resistance 15–30 Ω /Luminescence Technology, Taiwan) coated glass. The device area (\sim 0.1 cm²) was defined by the

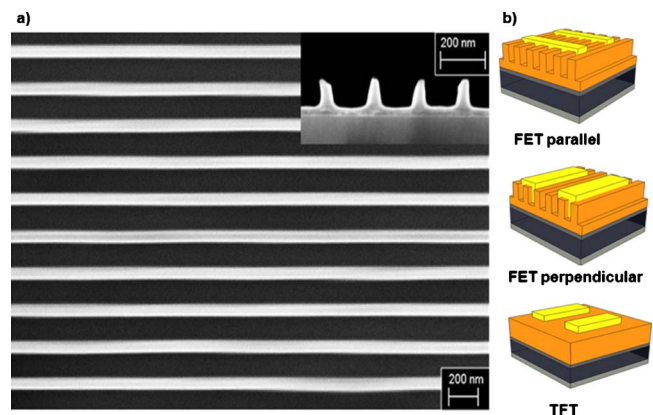


FIG. 2. (Color online) (a) Schematic of the nanograting field effect transistor with source and drain parallel and perpendicular to the nanogratings, and thin film transistor; (b) SEM image of P3HT nanogratings. The grating has 20 nm residual layer and 150–170 nm grating height.

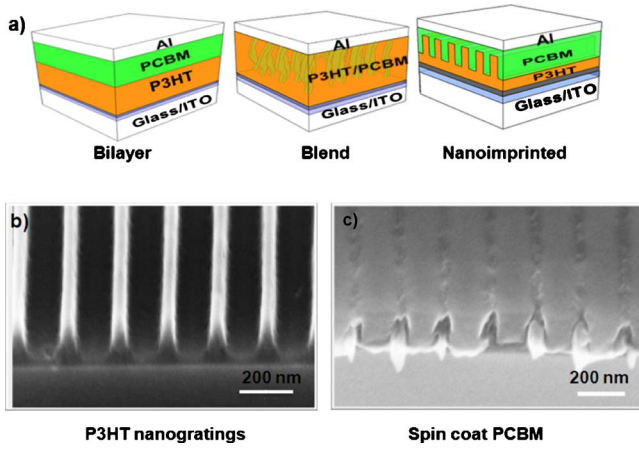


FIG. 3. (Color online) (a) Schematics of bilayer, blend, and nanograting solar cells; SEM images of P3HT nanogratings (b) before and (c) after infiltration of PCBM.

intersection of ITO and Al cathodes. First, a PEDOT:PSS layer or poly-3,4-ethylenedioxythiophene-polystyrene sulphonic acid (H. C. Starck, Inc.) mixed with d-sorbitol (Aldrich) was spin coated on the ITO substrates and dried in N_2 at $180^\circ C$ for 20 min. Then, an 85 nm thick P3HT film was spin casted on top of the PEDOT:PSS layer. Nanoimprinting was performed using a Si mold (gratings of 100 nm width, 100 nm depth, and 200 nm pitch) to form nanograting structures using similar NIL conditions as described for FETs. The resulting nanogratings have the same dimensions as the mold and a 30 nm thick residual layer. PCBM of 0.8 wt % in dichloromethane was spin casted as electron transfer material onto the imprinted P3HT nanogratings. Figure 3(b) shows scanning electron microscopy (SEM) images of P3HT nanogratings before and after infiltration of PCBM. We found that dichloromethane is an orthogonal solvent that dissolves PCBM well but not the P3HT, allowing the stacking of PCBM on top of the P3HT layer without distortion of the nanostructures.^{14,19} A thin LiF (3 nm) layer and 100 nm thick aluminum were thermally evaporated on the PCBM coated sample as the top electrode. The devices are characterized after annealing at $120^\circ C$ for 3 min. As a control study, a similar process was used to fabricate bilayer and blended nonpatterned solar cells without the imprint process. Figure 3(a) shows the schematic designs of bilayer, blend, and nanoimprinted OPV devices. The bilayer devices contain a 50 nm PCBM layer on top of an 85 nm thick P3HT layer, while the blend devices were made by spin coating an ~ 135 nm thick film of P3HT/PCBM blend (1:0.9) on a substrate. The devices were measured using Air Mass 1.5 global filtered solar simulated light (AM 1.5) calibrated using a Na-

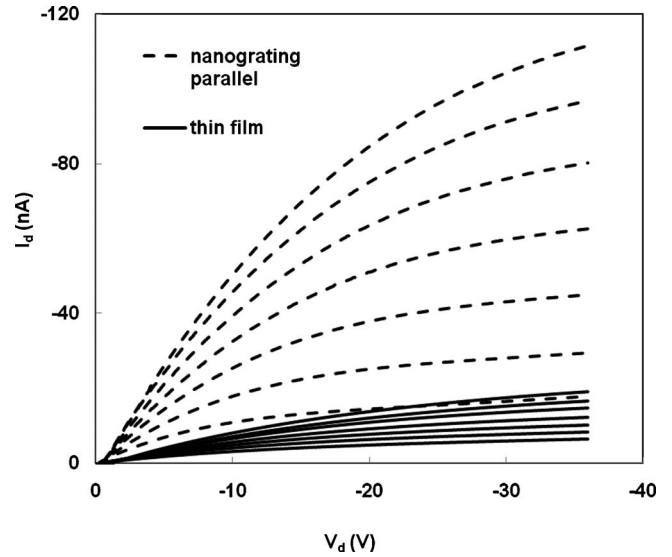


FIG. 4. I_{DS} vs V_{DS} characteristics of nanograting FET and TFT with effective channel length of $30 \mu m$, showing the accumulation mode operation when gate biases were applied from -5 to -35 V with an interval of -5 V.

tional Renewable Energy Laboratory certified silicon diode with a KG-5 color filter (Hamamatsu) at an intensity of 100 mW/cm^2 .

III. RESULTS AND DISCUSSIONS

Figure 4 shows drain current versus drain voltage (I_d - V_d) curves demonstrating typical FETs behavior with linear and saturation regions. Field effective mobilities are extracted according to

$$\frac{\partial I_d}{\partial V_g} = \frac{\mu_{FE} W C_i V_d}{L}, \quad (1)$$

where W , L , and C_i are the channel width, channel length, and gate capacitance, respectively.²⁰ In our devices, the channel length and width were 100 and $30 \mu m$, respectively. We intend to use the linear low-voltage region to calculate hole mobility, which is close to the biasing conditions of solar cells. The operation of solar cells can never be in the saturation or high-voltage region. From Fig. 4, the linear regions of the I_d - V_d curves stay below $V_d = -10$ V, thereby we fixed V_d at -5 V during I_d - V_g measurements. The mobility values were extracted using Eq. (1), where the value of G_M , i.e., $\partial I_d / \partial V_g$ was obtained from KEITHLY software.²¹ The calculated mobility values are shown in Tables I and II.

As expected, nanograting FETs show mobility values ($3.04 \times 10^{-2} \text{ cm}^2/\text{V s}$) 60 times higher than that of the TFT devices of 80 nm P3HT film ($5.62 \times 10^{-4} \text{ cm}^2/\text{V s}$). The

TABLE I. Hole mobility extracted from I - V curves of back-gated FETs for nanograting parallel, perpendicular, and thin film transistors, showing strong anisotropic conductivity in P3HT nanogratings.

Device	Parallel	Perpendicular	Thin film
Mobility ($\text{cm}^2/\text{V s}$)	$3.04 \times 10^{-2} \pm 3 \times 10^{-3}$	$5.48 \times 10^{-5} \pm 5 \times 10^{-6}$	$5.62 \times 10^{-4} \pm 5 \times 10^{-5}$

TABLE II. Hole mobility extracted from I - V curves of back-gated thin film transistors with different thicknesses, showing no dependence of hole mobility on the film thickness.

Thickness	20 nm	80 nm	140 nm
Mobility ($\text{cm}^2/\text{V s}$)	$4.67 \times 10^{-4} \pm 9.43 \times 10^{-5}$	$4.30 \times 10^{-4} \pm 1.25 \times 10^{-4}$	$5.24 \times 10^{-4} \pm 1.73 \times 10^{-4}$

P3HT thin film did not have any special treatment, such as surface treatment⁸ and electrospinning;⁷ therefore, the crystallinity of the film is low. The degree of crystallinity is significantly proportional to mobility values,¹⁵ so the TFT devices have much lower mobility compared to ordered nanograting FETs. The measured results also show a highly anisotropic conductance behavior in nanogratings: mobility along the grating direction is $3.04 \times 10^{-2} \text{ cm}^2/\text{V s}$, while mobility perpendicular to the grating direction is $5.11 \times 10^{-5} \text{ cm}^2/\text{V s}$. Moreover, mobility along the perpendicular direction is one order of magnitude lower than the thin film. Table II shows the TFT mobility values for three different thicknesses (20, 80, and 140 nm), and as we can see, the values are very close. It proves that the thin residual layer in perpendicular devices was not the reason for the low value of charge mobility of nanograting FETs in the perpendicular direction. P3HT conducts holes by a hopping mechanism and hopping rate decreases exponentially with increasing hopping distance,¹⁶ hence mobility parallel to the grating is expected to be significantly higher than in the perpendicular direction, as we observed experimentally. The mobility of P3HT depends on a number of other factors, such as polymer purity and high polydispersity, processing conditions, and measurement conditions.^{22–25} With specific film optimization and treatment, the reported mobility of P3HT can be as high as $\sim 0.1 \text{ cm}^2/\text{V s}$, which is higher than our results. However, they were measured under much higher drain voltage and in the saturation region, while our mobility is measured in the linear region under low voltages, which are the conditions for solar cell applications.²⁶

Hole mobility enhancement in P3HT nanogratings is due to nanoconfinement induced chain alignment in P3HT nanogratings defined by nanoimprint lithography, as shown in our previous work.¹⁷ In this highly ordered 3D grating structure, hopping distances of π - π stacking in the parallel direction and along the vertically aligned polymer backbones are about 3.8 \AA , while a hopping distance over the side chains is about 16.8 \AA in the perpendicular direction.¹⁷ This nanoconfinement induced ordering polymer chain is due to the combined effect of polymer flow at nearly molten state during the nanoimprinting and π - π interchain interaction and side chain hydrophobic interactions with hydrophobic mold walls. It has been shown that this directed organization goes up to tens of nanometers ($\sim 50 \text{ nm}$) for thin film P3HT contacting a substrate.⁹ Since the P3HT is confined in the mold cavity between two walls, this range would double. Such directed organization is likely incomplete when the channel width and/or the period of the nanograting mold is higher than the range of 100 nm . The nanograting size also affects polymer flow behavior to the nanochannels during nanoimprinting.

Therefore, such kind of chain alignment cannot be expected when large feature size nanogratings are used. Previously, Cui *et al.* used a 700 nm period grating mold with 50% duty cycle to improve the hole mobility of P3HT by NIL. They found a 12-fold increase in mobility from P3HT nanogratings compared to thin film. They observed that the carrier mobility in the perpendicular direction is two times that of the parallel direction, which is contradictory to our results.¹⁵ Their results are more likely due to pressure-induced crystallization for large period gratings rather than nanoconfinement induced polymer chain alignment and polymer flow behavior.^{27,28}

As described earlier, P3HT nanogratings exhibit a highly anisotropic conductance behavior: the mobility parallel to the grating direction is about 600 times as much as the perpendicular direction. This is due to highly ordered chain orientation in the grating structure: π - π stacking in the parallel direction with vertically aligned backbones.¹⁷ Since the hopping distance along π - π stacking and along the backbone is equal (3.8 \AA), the mobility along the vertical direction would be very close to the values parallel to the grating direction. So the field effective mobility calculated for the parallel direction can be a good estimate of the mobility in the vertical direction, which is the hole transport direction in solar cells. These results suggest that nanoimprinted solar cells would have higher hole carrier mobility than bulk heterojunction solar cells. The high mobility enabled by the favorable 3D chain configuration can contribute to the improved I_{sc} , FF, and efficiency of the nanoimprinted OPV solar cells. To prove this, nanograting OPV devices were fabricated and characterized.

I - V curves of bilayer, blended, and nanoimprinted OPV devices are plotted in Fig. 5, showing our preliminary results of using high density and ordered nanowires to make P3HT/

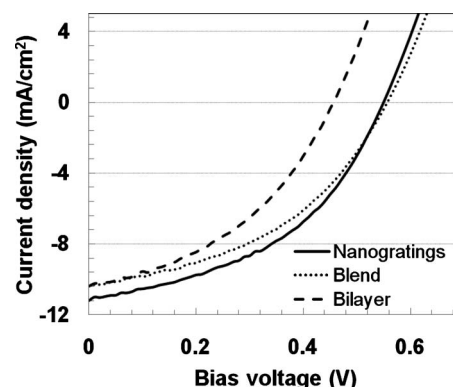


Fig. 5. I - V curves of bilayer, blend, and nanograting OPV devices.

TABLE III. Device characteristics for bilayer, blend, and nanograting solar cells, indicating improved power conversion efficiency by the nanograting device morphology.

Devices	Gratings	Blend	Bilayer
Voc (V)	0.55	0.56	0.46
Isc (mA/cm ²)	11.2	10.3	10.4
FF	0.45	0.43	0.41
η (%)	2.76	2.50	1.96

PCBM solar cells, and their device parameters are shown in Table III. The efficiency of nanoimprinted OPV is higher than bilayer and blend solar cells. Both FF and I_{sc} are higher in P3HT nanograting solar cells than the bilayer and blended counterparts. There can be two factors for this improved performance: increase in interface area and increase in charge mobility. The interface area of blend solar cells is the highest, but its I_{sc} is smaller than the nanograting devices, indicating that the hole mobility is enhanced in nanograting solar cells due to 3D chain alignment. On the other hand, the polymer crystallinity of bilayer solar cells can be better than in the nanostructures and blend devices, but it has the least interface area. Therefore, we believe that the improved performance in nanograting devices is partially due to the better chain alignment in P3HT nanogratings because high carrier mobility improves FF, external quantum efficiency, and I_{sc} .^{5,22,23} A significant increase in nanoimprinted solar cell performance can be expected by increasing the density and aspect ratio of nanogratings to increase the area of interface in addition to the enhancement of charge carrier mobility.

IV. CONCLUSIONS

We have shown that nanoimprint lithography is an effective way to enhance the charge carrier mobility of P3HT in field effect transistor and solar cells by inducing favorable 3D chain alignments in nanogratings. Nanoimprint also provides a precise nanostructuring method to shape heterojunctions so as to decrease the exciton travel length for charge dissociation, enhance charge transport and charge collection, and improve power conversion efficiency in OPV. In addition, polymer chain orientation in lithographically defined polymer nanogratings provides a unique platform to study correlations between morphology and transport mechanism for organic devices.

ACKNOWLEDGMENTS

This work is supported by the National Science Foundation (Grant No. ECCS-0901759), Welch Foundation Grant No. AT-1617, and CONTACT/AF consortium of Texas. M.Z. would like to thank UT Dallas for the get-doc fellowship.

- ¹V. D. Mihailetschi, H. X. Xie, B. de Boer, L. M. Popescu, J. C. Hummelen, P. W. M. Blom, and L. J. A. Koster, *Appl. Phys. Lett.* **89**, 012107 (2006).
- ²T. Aernouts, P. Vanlaeke, W. Geens, J. Poortmans, P. Heremans, S. Borghs, R. Mertens, R. Andriessen, and L. Leenders, *Thin Solid Films* **451–452**, 22 (2004).
- ³A. L. Briseno, S. C. B. Mannsfeld, S. A. Jenekhe, Z. Bao, and Y. Xia, *Mater. Today* **11**, 38 (2008).
- ⁴S. R. Forrest, *MRS Bull.* **30**, 28 (2005).
- ⁵S. E. Shaheen, C. J. Brabec, N. S. Sariciftci, F. Padinger, T. Fromherz, and J. C. Hummelen, *Appl. Phys. Lett.* **78**, 841 (2001).
- ⁶A. Gadisa, F. L. Zhang, D. Sharma, M. Svensson, M. R. Andersson, and O. Inganäs, *Thin Solid Films* **515**, 3126 (2007).
- ⁷J. Park, S. Lee, and H. H. Lee, *Org. Electron.* **7**, 256 (2006).
- ⁸S. Lee, G. D. Moon, and U. Jeong, *J. Mater. Chem.* **19**, 743 (2009).
- ⁹R. J. Kline, M. D. McGehee, and M. F. Toney, *Nature Mater.* **5**, 222 (2006).
- ¹⁰D. E. Motaung, G. F. Malgas, C. J. Arendse, S. E. Mavundla, C. J. Oliphant, and D. Knoesen, *J. Mater. Sci.* **44**, 3192 (2009).
- ¹¹Y. Zhao, Z. Y. Xie, Y. Qu, Y. H. Geng, and L. X. Wang, *Appl. Phys. Lett.* **90**, 043504 (2007).
- ¹²I. McCulloch, *Nature Mater.* **4**, 583 (2005).
- ¹³Z. J. Hu, G. Baralia, V. Bayot, J. F. Gohy, and A. M. Jonas, *Nano Lett.* **5**, 1738 (2005).
- ¹⁴M. Aryal, F. Buyukserin, K. Mielczarek, X.-M. Zhao, J. Gao, A. Zakhdov, and W. Hu, *J. Vac. Sci. Technol. B* **26**, 2562 (2008).
- ¹⁵D. Cui, H. Li, H. Park, and X. Cheng, *J. Vac. Sci. Technol. B* **26**, 2404 (2008).
- ¹⁶Z. J. Hu, B. Muls, L. Gence, D. A. Serban, J. Hofkens, S. Melinte, B. Nysten, S. Demoustier-Champagne, and A. M. Jonas, *Nano Lett.* **7**, 3639 (2007).
- ¹⁷M. Aryal, K. Trivedi, and W. Hu, *ACS Nano* **3**, 3085 (2009).
- ¹⁸H. P. Jia, G. K. Pant, E. K. Gross, R. M. Wallace, and B. E. Gnade, *Org. Electron.* **7**, 16 (2006).
- ¹⁹A. L. Ayzner, C. J. Tassone, S. H. Tolbert, and B. J. Schwartz, *J. Phys. Chem. C* **113**, 20050 (2009).
- ²⁰E. von Hauff, V. Dyakonov, and R. Parisi, *Sol. Energy Mater. Sol. Cells* **87**, 149 (2005).
- ²¹H. Q. Liu, C. H. Reccius, and H. G. Craighead, *Appl. Phys. Lett.* **87**, 253106 (2005).
- ²²R. J. Kline, M. D. McGehee, E. N. Kadnikova, J. S. Liu, J. M. J. Fréchet, and M. F. Toney, *Macromolecules* **38**, 3312 (2005).
- ²³J. A. Merlo and C. D. Frisbie, *J. Phys. Chem. B* **108**, 19169 (2004).
- ²⁴M. L. Chabiny, R. A. Street, and J. E. Northrup, *Appl. Phys. Lett.* **90**, 123508 (2007).
- ²⁵K. Norrman, A. Ghanbari-Siahkali, and N. B. Larsen, *Annu. Rep. Prog. Chem., Sect. C: Phys. Chem.* **101**, 174 (2005).
- ²⁶Y. Fu, C. Lin, and F.-Y. Tsai, *Org. Electron.* **10**, 883 (2009).
- ²⁷H. D. Rowland, W. P. King, J. B. Pethica, and G. L. W. Cross, *Science* **322**, 720 (2008).
- ²⁸C. F. Shih, K. T. Hung, J. W. Wu, C. Y. Hsiao, and W. M. Li, *Appl. Phys. Lett.* **94**, 143505 (2009).